

Current convective instability in detached divertor plasma

S. I. Krasheninnikov, and A. I. Smolyakov

Citation: *Physics of Plasmas* **23**, 092505 (2016); doi: 10.1063/1.4962568

View online: <https://doi.org/10.1063/1.4962568>

View Table of Contents: <http://aip.scitation.org/toc/php/23/9>

Published by the *American Institute of Physics*

Articles you may be interested in

[Divertor plasma detachment](#)

Physics of Plasmas **23**, 055602 (2016); 10.1063/1.4948273

[Impurity-induced divertor plasma oscillations](#)

Physics of Plasmas **23**, 012503 (2016); 10.1063/1.4939539

[Attainment of a stable, fully detached plasma state in innovative divertor configurations](#)

Physics of Plasmas **24**, 056112 (2017); 10.1063/1.4979193

[On detachment asymmetry and stability](#)

Physics of Plasmas **24**, 072508 (2017); 10.1063/1.4991402

[Macroscopic motion of sheath-connected blobs in magnetic fields with arbitrary topology](#)

Physics of Plasmas **24**, 012301 (2017); 10.1063/1.4972800

[Finite-Resistivity Instabilities of a Sheet Pinch](#)

The Physics of Fluids **6**, 459 (1963); 10.1063/1.1706761

**COMPLETELY
REDESIGNED!**



**PHYSICS
TODAY**

Physics Today Buyer's Guide
Search with a purpose.

Current convective instability in detached divertor plasma

S. I. Krasheninnikov¹ and A. I. Smolyakov²

¹University California San Diego, 9500 Gilman Drive, La Jolla, California 92093-0411, USA

²University of Saskatchewan, 116 Science Place, Saskatoon, Saskatchewan S7N 5E2, Canada

(Received 13 May 2016; accepted 29 August 2016; published online 14 September 2016)

The asymmetry of inner and outer divertors, which cause the inner divertor to detach first, while the outer one is still attached, results in the large temperature difference between the vicinities of inner and outer targets and the onset of large electric potential drop through detached plasma of the inner divertor. A large potential drop along with the inhomogeneity of the resistivity of detached plasma across the divertor leg drives the current convective instability in the inner divertor and subsequent fluctuations of radiation loss similar to that observed in experiments. The estimates of the frequency of plasma parameter fluctuations due to the current convective instability are in a reasonable agreement with experimental data. Once the outer divertor also detaches, the temperature difference between the vicinities of inner and outer targets disappears, and the driving force for the current convective instability, and resulting oscillations of radiation loss, vanishes. This feature is indeed observed in experiments. *Published by AIP Publishing.*

[<http://dx.doi.org/10.1063/1.4962568>]

I. INTRODUCTION

Large heat and particle fluxes on divertor targets, envisioned in magnetic fusion reactors, make the detached regime of divertor operation in future reactors virtually mandatory. Therefore, it is very important to have a clear understanding of both transition to the detached regime and the physics of the detached plasma. Detached divertor regimes are characterized by large radiation loss, reduction of plasma flux to the targets, and cold recombining plasma in significant part of divertors.¹ Experimental data show that the transition to detachment can have bifurcation-like character, while the operation in the detached regime can exhibit rather strong fluctuations of the radiation loss and enhanced cross-field plasma transport (e.g., see Refs. 2–5). Although simplified analytical models and numerical simulations demonstrate the possibilities of such phenomena (e.g., see Refs. 6–8 and the references therein), the physics of experimentally observed bifurcations and fluctuations is still not clear.

In this paper, we present a plausible explanation of origin of radiation fluctuations in the AUG tokamak reported in Ref. 3. These fluctuations, with the frequencies ~ 10 kHz, were observed for the case where only the inner divertor was detached and both the detachment and radiation fronts were located close to the X-point. However, radiation fluctuations disappear when the outer divertor also detaches.

We show that the origin of the radiation oscillations can be attributed to current convective instability⁹ developing in the cold plasma in the inner divertor. It is widely accepted that current convective instability, which in the tokamak related literature also called “rippling mode” (e.g., see Refs. 10–12), does not play a significant role in anomalous plasma transport in the hot core region due to the high plasma heat conduction along the magnetic field and the magnetic shear effect,¹³ although it might be important in relatively cold edge plasma.^{11,12} However, on the closed flux surfaces, the parallel electric field driving the parallel current causing the

rippling instability is small, $\sim 10^{-3}$ V/cm, while in the scrape off layer (SOL) plasma (see Fig. 1), it can be much larger, ~ 1 V/cm. The reason for this is that in the SOL, the parallel current is largely driven by the difference of electron temperatures $T_d^{(out)}$ and $T_d^{(in)}$ in the vicinity of outer and inner divertor targets, respectively.¹⁴ This is because the drop of electrostatic potential through the sheath is $\sim 4T_d$ for the case where no current flows through the sheath. For the case where $T_d^{(out)} \neq T_d^{(in)}$ and inner and outer divertor targets are electrically connected (which is the case in current tokamaks), the current will flow through the SOL plasma. The magnitude of the current will be determined by the difference $T_d^{(out)} - T_d^{(in)}$ and the SOL plasma resistivity.¹⁴ When the inner (outer) divertor is detached (attached), we have $T_d^{(out)} \gg T_d^{(in)}$ and the SOL resistivity is largely determined by the resistivity of cold, ~ 1 eV, plasma in the inner divertor. As a result, virtually the whole potential drop, $U \sim 4T_d^{(out)}$, driving the SOL current will be localized within the detached plasma, creating a large parallel electric field. This high electric field in the

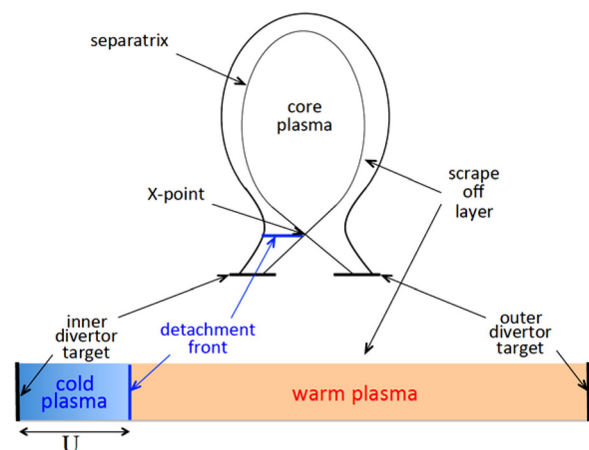


FIG. 1. Schematic view of the poloidal cross-section of a tokamak and a scrape off layer shown in a straight flux tube approximation.

SOL, in conjunction with a very low plasma temperature in the detached divertor region, which strongly decreases the stabilizing role of electron heat conduction, can cause robust current convective instability in the detached plasma.

Fluctuation of plasma parameters, including pressure, in the detached inner divertor will cause the bursts of plasma outflow from the radiation region (located beyond the detachment front) towards the target and subsequent fluctuation of the radiation losses. Once the outer divertor also detaches, a strong asymmetry between $T_d^{(out)}$ and $T_d^{(in)}$, causing a large potential drop through the inner divertor, disappears. As a result, when both divertors are detached, the drive for the current convective instability in the inner divertor and the subsequent fluctuations of the radiation losses do not exist anymore. This qualitative physical picture agrees with experimental observations.³ We will show later in the paper that the expected frequency range of current convective instability is also consistent with the experimental data.

The rest of the paper is organized as follows: in Section II, we discuss and justify the simplified physical model of a detached plasma we will be using here, and present the governing equation describing the current convective instability as well as some important estimates of the growth rate, characteristic wavelengths, and the instability threshold; in Section III, we analyze and solve this equation and find the conditions for current convective instability and corresponding growth rate. In Section IV, we summarise the results and compare them with the available experimental observations.

II. PHYSICAL MODEL

We will consider a slab approximation for a detached inner divertor plasma assuming periodic boundary conditions along the ‘‘toroidal’’ z -coordinate (see Fig. 2). In the poloidal direction ($T_{cold} \sim \text{few eV}$, we assume that electron and ion temperatures are equal), the cold plasma region extends at the distance $L_\perp \sim 10 \text{ cm}$ up to the detachment front where it contacts with warm ($\sim \text{few tens of eV}$) SOL plasma. The characteristic scale-length of temperature and, therefore, conductivity variation along ‘‘radial’’ coordinate x we assume $a \sim 2 \text{ cm}$. We assume the potential drop, U , between the detachment front and the target, to be $eU \equiv U_e \sim 4T_d^{(out)} \sim 30 \text{ eV} \gg T_{cold} \sim 3 \text{ eV}$, where e is the electron charge. In our estimates, we will assume that the plasma density in the detached region, $n_{det} \sim 3 \times 10^{14} \text{ cm}^{-3}$, the magnitude of

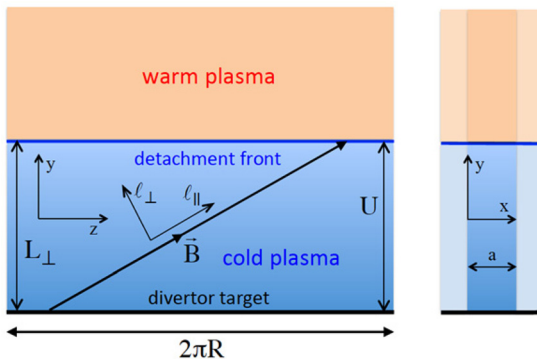


FIG. 2. Schematic view of the inner divertor plasma in a slab approximation.

magnetic fields $B_z \sim 3 \text{ T}$ and $B_y \sim 0.1 \times B_z$, and the effective magnetic shear length $L_s \sim 1 \text{ m}$ (we assume that the detachment front is not too close to the X-point where the magnetic shear is much stronger).

First, we notice that the potential drop through the detached plasma causes $E \times B$ drift in the radial direction. As a result, the detached plasma parameters are determined by two competing processes: radial $E \times B$ drift, which is characterized by the frequency $\nu_{E \times B}^{(x)} \approx (U_e/M)/(\Omega_i a L_\perp)$ (where M and Ω_i are the ion mass and gyro-frequency) and parallel plasma flow having a characteristic time-scale $\tau_\parallel \approx L_\perp/(b_y \sqrt{T_{cold}/M})$, where $\vec{b} = \vec{B}/B$ ($b_z^2 \gg b_y^2$) and $L_\parallel = L_\perp/|b_y| \sim 1 \text{ m}$. For the parameters of the interest, we have $\tau_\parallel \nu_{E \times B}^{(x)} \approx 0.3 \lesssim 1$, so that in a ballpark we can assume rather well defined kernel of the detached plasma layer with electron temperature and, therefore, electric conductivity significantly different from the surrounding plasma, which is shown in light blue color in Fig. 2.

Then, neglecting the effects of parallel electron heat conduction (corresponding estimates will be given below) and taking the parallel electric current $J_\parallel = \sigma_0(x)E_\parallel$ and perpendicular one determined by ion inertia, from $\nabla \cdot \vec{J} = 0$, we find the following linearized equation for electrostatic potential $\Phi \propto \varphi(\vec{r})e^{-i\omega t}$ describing the current-convective instability:

$$\frac{\omega}{\omega_A} \nabla_\perp^2 \varphi + i \nabla_\parallel \left\{ \frac{\omega_\sigma}{\omega} (\vec{e}_x \times \vec{b}) \cdot \nabla + \nabla_\parallel \right\} \varphi = 0, \quad (1)$$

where $\omega_A = 4\pi\sigma_0(V_A/c)^2$, $\omega_\sigma = -i(cE_\parallel/B)[d\ln(\sigma_0)/dx]$, $E_\parallel = U_e/(eL_\parallel)$ is the parallel component of electric field, $\sigma_0(x)$ is the plasma electric conductivity determined by electron temperature ($\sim 3 \text{ eV}$) of detached plasma, and c and $V_A = B/\sqrt{4\pi Mn_{det}}$ are the light and the Alfvén speeds, respectively. We notice that for the parameters of interest $\omega_A \sim 10^{11} \text{ s}^{-1} \gg |\omega_\sigma| \sim 10^3 \text{ s}^{-1}$ (we assume here that $|d\ln(\sigma_0)/dx| \approx 2/a$).

Generally speaking, frequency ω should be found as an eigenvalue of the solution of Eq. (1). Therefore, we need to specify the boundary conditions for the function $\varphi(\vec{r})$. We will assume $\varphi(|x| \rightarrow \infty) \rightarrow 0$ and the periodic boundary conditions along the z -coordinate $(\dots)_{z=0} = (\dots)_{z=2\pi R}$. To find the boundary conditions for $\varphi(\vec{r})$ at the target ($y=0$) and at the detachment front ($y=L_\perp$), we take into account that: (i) The resistivity of warm plasma beyond the detachment front is much larger than the resistivity of the cold detached plasma in the inner divertor; (ii) on the other hand, effective sheath resistivity becomes smaller than the resistivity of the detached plasma if $\lambda_C/L_\parallel < \sqrt{m_e/M}$ ¹⁵ (here, λ_C is the coulomb mean free path and m_e is the electron mass). For the parameters of interests, we have $\lambda_C/L_\parallel \sim 10^{-3} \ll \sqrt{m_e/M} \approx 2 \times 10^{-2}$ and an impact of effective sheath resistivity, which could be responsible for some specific plasma instabilities (e.g., see Refs. 15 and 16), can be ignored. As a result, we can apply the following boundary conditions: $\varphi_{y=0} = \varphi_{y=L_\perp} = 0$.

Before going into detail analysis of the solution of Eq. (1), we consider it by using the eikonal approximation assuming $\varphi(\vec{r}) \propto \exp(ik_\perp \ell_\perp + ik_\parallel \ell_\parallel + ik_x x)$, where the coordinates ℓ_\perp and ℓ_\parallel are shown in Fig. 2, while k_\perp , k_\parallel , and

k_x are the corresponding wave numbers. Then, from Eq. (1), we find the following dispersion equation:

$$-i \frac{\omega}{\omega_A} \frac{k_\perp^2 + k_x^2}{k_\parallel^2} + \frac{\omega_\sigma k_\perp}{\omega k_\parallel} + 1 = 0. \quad (2)$$

First, we consider the case $k_x = 0$. Then, from Eq. (2), we find that for $|k_\perp/k_\parallel| < (\omega_A/|\omega_\sigma|)^{1/3}$, the first term in Eq. (1) can be neglected and the growth rate of the instability, γ , increases with increasing $|k_\perp/k_\parallel|$ as

$$\omega = i\gamma = i \left| \omega_\sigma \frac{k_\perp}{k_\parallel} \right| \quad (3)$$

reaches the maximum value

$$\gamma \approx |\operatorname{Re}(\omega)| \approx \omega_{\max}^{(A)} \equiv (\omega_A |\omega_\sigma|)^{1/3} \quad (4)$$

at $|k_\perp/k_\parallel| \approx |k_\perp/k_\parallel|_{\max}^{(A)} \equiv (\omega_A/|\omega_\sigma|)^{1/3}$, when all terms in Eq. (1) are of the same order, and then decreases with increasing $|k_\perp/k_\parallel| > |k_\perp/k_\parallel|_{\max}^{(A)}$ as

$$\gamma \approx |\operatorname{Re}(\omega)| \approx \left(\frac{\omega_A |\omega_\sigma|}{|k_\perp/k_\parallel|} \right)^{1/3}. \quad (5)$$

In this limit, only the first and second terms in Eq. (1) matter. Thus, we see that for the parameters of interest, the maximum growth rate is of the order of $\omega_{\max}^{(A)} \sim 5 \times 10^5 \text{ s}^{-1}$. However, so far, we neglected the stabilizing effect of parallel electron heat conduction, which can flatten electron temperature and, therefore, electric conductivity perturbation driving instability. This is only valid (e.g., see Refs. 10 and 13 and the references therein) for $\gamma > \alpha_e k_\parallel^2$, where $\alpha_e = (2/3)(\kappa_e/n_{\text{det}})$ is the electron heat diffusivity. However, taking as an estimate of the smallest $|k_\parallel| \approx 2\pi/L_\parallel$, we find that $\alpha_e k_\parallel^2 \sim 2 \times 10^4 \text{ s}^{-1} \ll \omega_{\max}^{(A)}$ and the instability cannot be stabilized by parallel electron heat conductivity. As a matter of fact, from Eq. (3), we find that the threshold for the instability is determined by the inequality

$$(k_\perp)_{\text{thr}} \gtrsim \alpha_e k_\parallel^3 / |\omega_\sigma|, \quad (6)$$

which for $|k_\parallel| \approx 2\pi/L_\parallel$ corresponds to $(\lambda_\perp)_{\text{thr}} = 2\pi(k_\perp)_{\text{thr}}^{-1} \gtrsim 5 \text{ cm}$. We also notice that for the parameters of interest $\lambda_{\max} \sim 0.2 \text{ cm}$ ($\lambda_{\max}^{(A)} = 2\pi/(k_\perp)_{\max}^{(A)}$) and $|(k_\perp)_{\max}| \rho_i(T_{\text{cold}}) \sim 0.1 \ll 1$, where $\rho_i(T_{\text{cold}})$ is the ion gyro-radius for ion temperature T_{cold} , so that the finite Larmor radius effects can also be ignored.

Let us now discuss an impact of k_x . Based on the preceding analysis, we find that within the eikonal approximation, any sizable effect of k_x on the growth rate is possible for $k_x^2 \gtrsim (k_\perp)_{\max}^{(A)}$. Estimating $k_x \approx (2\pi/a)^2$ and noticing that $\lambda_{\max}^{(A)} \sim 0.2 \text{ cm} \ll a \sim 2 \text{ cm}$, we conclude that within a long wavelength eikonal approximation k_x does not alter the results of our analysis of the instability growth rate.

III. SOLUTION OF GOVERNING EQUATION

Unfortunately, we are not able to solve Eq. (1) and find ω as an eigenvalue of the solution. Therefore, first we will

find the solution of Eq. (1) and proper boundary conditions on the (y, z) plane assuming that $\varphi(\vec{r}) = \varphi(y, z) \exp(ik_x^{\text{eff}}x)$, where k_x^{eff} is some effective wave number.

Then, expanding $\varphi(z, y)$ in the Fourier series $\varphi(z, y) = \sum_n \varphi_n(y) \exp(ik_n z)$, where $k_n = n/R$, from Eq. (1), we find

$$\begin{aligned} & \frac{\omega}{\omega_A} \left\{ \left(b_z \frac{\partial}{\partial y} - ik_n b_y \right)^2 - (k_x^{\text{eff}})^2 \right\} \varphi_n \\ & + i \left(b_y \frac{\partial}{\partial y} + ik_n b_z \right) \left\{ \frac{\omega_\sigma}{\omega} \left(b_z \frac{\partial}{\partial y} - ik_n b_y \right) \right. \\ & \left. + \left(b_y \frac{\partial}{\partial y} + ik_n b_z \right) \right\} \varphi_n = 0. \end{aligned} \quad (7)$$

Taking $\varphi_n(y) \propto \exp(\eta y)$, we find the following equation for η :

$$\eta^2 f_2 + \eta f_1 + f_0 = 0, \quad (8)$$

where

$$\begin{aligned} f_2 &= \frac{\omega}{\omega_A} b_z^2 + i \left(\frac{\omega_\sigma}{\omega} b_z + b_y \right) b_y \\ f_1 &= \left\{ \frac{\omega}{\omega_A} 2ib_z b_y - \frac{\omega_\sigma}{\omega} (b_z^2 - b_y^2) - 2b_z b_y \right\} k_n \\ f_0 &= \left\{ -\frac{\omega}{\omega_A} \left(b_y^2 + \frac{(k_x^{\text{eff}})^2}{k_n^2} \right) + i \left(\frac{\omega_\sigma}{\omega} b_z b_y - b_z^2 \right) \right\} k_n^2. \end{aligned} \quad (9)$$

As a result, we have

$$\eta_{(\pm)} = -\frac{f_1}{2f_2} \pm \left\{ \left(\frac{f_1}{2f_2} \right)^2 - \frac{f_0}{f_2} \right\}^{1/2}, \quad (10)$$

and can express $\varphi_n(y)$ as follows:

$$\varphi_n(y) = \varphi_n^{(+)} \exp(\eta_{(+)} y) + \varphi_n^{(-)} \exp(\eta_{(-)} y), \quad (11)$$

where $\varphi_n^{(+)}$ and $\varphi_n^{(-)}$ are some constants. Then, from the boundary conditions $\varphi_n(y=0) = \varphi_n(y=L_\perp) = 0$, we find $\varphi_n^{(+)} = -\varphi_n^{(-)}$ and arrive to the following equation for the eigenvalue ω :

$$2 \left\{ \left(\frac{f_1}{f_2} \right)^2 - \frac{f_0}{f_2} \right\}^{1/2} = i \frac{2\pi m}{L_\perp} \equiv ik_m, \quad (12)$$

where m is the integer number. Using expressions (9), we can re-cast Eq. (12) as

$$\begin{aligned} & \frac{1}{4} \left\{ \frac{\frac{\omega}{\omega_A} 2ib_z b_y - \frac{\omega_\sigma}{\omega} (b_z^2 - b_y^2) - 2b_z b_y}{\frac{\omega}{\omega_A} b_z^2 + i \left(\frac{\omega_\sigma}{\omega} b_z + b_y \right) b_y} \right\}^2 \\ & - \frac{\frac{\omega}{\omega_A} \left(b_y^2 + \frac{(k_x^{\text{eff}})^2}{k_n^2} \right) + i \left(\frac{\omega_\sigma}{\omega} b_z b_y - b_z^2 \right) b_z}{\frac{\omega}{\omega_A} b_z^2 + i \left(\frac{\omega_\sigma}{\omega} b_z + b_y \right) b_y} = -\frac{1}{4} \frac{k_m^2}{k_n^2}. \end{aligned} \quad (13)$$

We start our analysis of Eq. (13) assuming that $\omega \ll \omega_A$. Then, simplified Eq. (13) gives

$$\left\{ \frac{\omega_\sigma (b_z^2 - b_y^2) + 2b_z b_y}{\left(\frac{\omega_\sigma}{\omega} b_z + b_y \right) b_y} \right\}^2 + 4 \frac{\left(\frac{\omega_\sigma}{\omega} b_y - b_z \right) b_z}{\left(\frac{\omega_\sigma}{\omega} b_z + b_y \right) b_y} = \frac{k_m^2}{k_n^2}. \quad (14)$$

From Eq. (14), we find

$$\frac{\omega_\sigma}{\omega} = g_{m,n} \pm \left\{ (g_{m,n})^2 + \frac{b_y}{b_z} g_{m,n} \right\}^{1/2}, \quad (15)$$

where

$$g_{m,n} = \frac{b_y^3 b_z (k_m/k_n)^2}{1 - (b_y b_z)^2 (k_m/k_n)^2}. \quad (16)$$

From Eq. (15), we see that for $|g_{m,n}| \lesssim |b_y/b_z|$, which corresponds to $(b_y b_z)^2 (k_m/k_n)^2 \lesssim 1$, the growth rate decreases as

$$\omega = i|\omega_\sigma| \left\{ |b_y/b_z| g_{m,n} \right\}^{-1/2} \cong i \left| \frac{\omega_\sigma}{b_y} \right| \left| \frac{k_n}{b_y k_m} \right| \gtrsim i \left| \frac{\omega_\sigma}{b_y} \right|, \quad (17)$$

with increasing $|g_{m,n}|$ and saturates at

$$\omega = i|\omega_\sigma| |b_z/b_y|, \quad (18)$$

for $|g_{m,n}| \gtrsim |b_y/b_z|$.

To get some insights in expression (17) and to compare it with the results of Section II, let us evaluate effective $(k_{\parallel}^2)_{\text{eff}} = |b_y \eta_{(\pm)} + i b_z k_n|^2$ and $(k_{\perp}^2)_{\text{eff}} = |b_z \eta_{(\pm)} - i b_y k_n|^2$. Estimating $\eta_{(\pm)}$ from Eq. (10) and taking into account Eq. (12), we find

$$\eta_{(\pm)} = -i \frac{\omega_\sigma (b_z^2 - b_y^2) + 2b_z b_y}{2 \left(\frac{\omega_\sigma}{\omega} b_z + b_y \right) b_y} k_n \pm i \frac{k_m}{2}. \quad (19)$$

For the most interesting case of large growth rate, $(b_y b_z)^2 (k_m/k_n)^2 \gtrsim 1$, using Eq. (17), we find

$$\eta_{(\pm)} = -i \left(\frac{b_z}{b_y} - \frac{1}{2b_y^2} \frac{\omega_\sigma}{\omega} \right) k_n \pm i \frac{k_m}{2} = -i \frac{b_z}{b_y} k_n + i \delta_m k_m, \quad (20)$$

where $|\delta_m| \sim 1$. We notice that under conditions of interest, $(b_y b_z)^2 (k_m/k_n)^2 \gtrsim 1$, the term $-i(b_z/b_y)k_n$ dominates in Eq. (15), which keeps effective parallel wave number, $(k_{\parallel})_{\text{eff}}$, small and effective perpendicular wave number, $(k_{\perp})_{\text{eff}}$, large. As a result, we have

$$\left(k_{\parallel}^2 \right)_{\text{eff}} \cong (b_y k_m)^2, \quad \left(k_{\perp}^2 \right)_{\text{eff}} \cong (b_z^2/b_y)^2 k_n^2 \gg \left(k_{\parallel}^2 \right)_{\text{eff}}. \quad (21)$$

Therefore, expression (17) can be written in a way similar to Eq. (3)

$$\omega = i\gamma = i \left| \omega_\sigma \frac{(k_{\perp})_{\text{eff}}}{(k_{\parallel})_{\text{eff}}} \right|. \quad (22)$$

In order to keep stabilizing impact of the parallel electron heat conduction small, we should take $m = 1$, which gives $(k_{\parallel}^2)_{\text{eff}} \cong (b_y 2\pi/L_{\perp})^2 = (2\pi/L_{\parallel})^2$ as we have estimated in Section I. Thus, we see that our eigenvalue/eigenfunction solution of Eq. (1) on the (y, z) plane gives us virtually the same dependencies for the growth rate of the instability as the eikonal approximation does.

Let us now consider how nonlocal effects in the x -direction can alter our eikonal approximation results. As in Section I, we will assume that $\varphi(\vec{r}) = \varphi(x) \exp(i k_{\perp} \ell_{\perp} + i k_{\parallel} \ell_{\parallel})$ and adopt the following dependence of plasma conductivity:

$$\sigma_0(x) = \begin{cases} \bar{\sigma}_0, & \text{for } |x| > a/2 \\ \bar{\sigma}_0 + \Delta \bar{\sigma}_0 (1 - 2|x|/a), & \text{for } |x| < a/2. \end{cases} \quad (23)$$

Then, assuming $\Delta \bar{\sigma}_0 \ll \bar{\sigma}_0$, from Eq. (1) we find the following equation for $\varphi(x)$:

$$\frac{\omega}{\omega_A} \left(\frac{d^2}{dx^2} - k_{\perp}^2 \right) \varphi - i k_{\parallel}^2 \left\{ \text{sign}(x) \frac{\tilde{\omega}_\sigma k_{\perp}}{\omega k_{\parallel}} (1 - H(1 - 2|x|/a)) + 1 \right\} \varphi = 0, \quad (24)$$

where $\tilde{\omega}_\sigma = i(\Delta \bar{\sigma}_0 / \bar{\sigma}_0)(2cE_{\parallel}/Ba)$, $\text{sign}(x) = x/|x|$ and $H(x)$ is the Heaviside function. One can easily see that the solution of Eq. (24) with the boundary conditions $\varphi(|x| \rightarrow \infty) \rightarrow 0$ can be written in a piecewise form

$$\varphi(x) = \begin{cases} \varphi_{(+)} \exp(-k_0(x - a/2)), & \text{for } x > a/2 \\ \varphi_{(++)} \exp(k_{(+)x}) + \varphi_{(+-)} \exp(-k_{(+)x}), & \text{for } 0 < x < a/2 \\ \varphi_{(-+)} \exp(k_{(-)x}) + \varphi_{(--)} \exp(-k_{(-)x}), & \text{for } -a/2 < x < 0 \\ \varphi_{(-)} \exp(k_0(x + a/2)), & \text{for } x < -a/2, \end{cases} \quad (25)$$

where

$$\begin{aligned} k_0^2 &= k_\perp^2 + ik_\parallel^2 \frac{\omega_A}{\omega} (\text{Re}(k_0) > 0) \quad \text{and} \\ k_{(\pm)}^2 &= k_0^2 \pm i \frac{\tilde{\omega}_\sigma \omega_A}{\omega^2} k_\parallel k_\perp, \end{aligned} \quad (26)$$

while the constants $\varphi_{(+)}$, $\varphi_{(++)}$, $\varphi_{(+-)}$, $\varphi_{(-)}$, $\varphi_{(-)}$, and $\varphi_{(-)}$ should be found from the continuity of both $\varphi(x)$ and its derivative. As a result, after some algebra, we arrive to the following dispersion equation:

$$\begin{aligned} &(1 + \chi_{(+)}) (1 - \chi_{(-)}) (\chi_{(+)} - \chi_{(-)}) \exp\{(k_{(+)} - k_{(-)})a/2\} \\ &- (1 + \chi_{(+)}) (1 + \chi_{(-)}) (\chi_{(+)} + \chi_{(-)}) \exp\{(k_{(+)} + k_{(-)})a/2\} \\ &+ (1 - \chi_{(+)}) (1 - \chi_{(-)}) (\chi_{(+)} + \chi_{(-)}) \exp\{-(k_{(+)} + k_{(-)})a/2\} \\ &- (1 - \chi_{(+)}) (1 + \chi_{(-)}) (\chi_{(+)} - \chi_{(-)}) \exp\{-(k_{(+)} - k_{(-)})a/2\} = 0, \end{aligned} \quad (27)$$

where $\chi_{(\pm)} = k_{(\pm)}/k_0$. By analyzing Eq. (27), we find that taking $k_{(+)} = i4\pi j_{(+)} / a \equiv ik_{(+)}^{\text{eff}}$ ($k_{(-)} = i4\pi j_{(-)} / a \equiv ik_{(-)}^{\text{eff}}$) and assuming $\text{Re}(k_{(-)})a/2 \gg 1$ ($\text{Re}(k_{(+)})a/2 \gg 1$), where $j_{(+)}$, ($j_{(-)}$) is some integer number results, for the case $|k_{(\pm)}^{\text{eff}}/k_\parallel| \lesssim |k_\perp/k_\parallel|_{\text{max}}$, in the cancelation of all leading order terms in Eq. (27) and the dispersion equation similar to Eq. (2)

$$-i \frac{\omega}{\omega_A} \frac{k_\perp^2 + (k_{(\pm)}^{\text{eff}})^2}{k_\parallel^2} \pm \frac{\tilde{\omega}_\sigma k_\perp}{\omega k_\parallel} + 1 = 0. \quad (28)$$

Thus, the growth rate of the instability in nonlocal approximation in the x -direction for the case where we can neglect the first term in Eq. (28) is

$$\omega = i\gamma = i \left| \tilde{\omega}_\sigma \frac{k_\perp}{k_\parallel} \right|. \quad (29)$$

This is not surprising since in this case, where $\text{Re}(k_{(-)})a/2 \gg 1$ and $\text{Re}(k_{(+)})a/2 \gg 1$, we could use an eikonal approximation, which would result in a local dispersion equation (2). We notice that the opposite case $|k_{(\pm)}|a/2 \ll 1$ has a very small applicability range.

Let now discuss an impact of the shear of the magnetic field on current convective instability. As we have mentioned above, both spatial localization and the growth rate of the ‘‘rippling mode’’ crucially depend on magnetic shear.^{10–13} However, while for the ‘‘rippling mode’’ developing on some closed rational magnetic flux surface, the effective length of the magnetic field line and, therefore, the stabilizing effect of parallel heat conduction are determined solely by the magnetic shear, in our case the length of the magnetic field line between the target and detachment front does not vary much. Indeed, assuming that $b_y(x) = b_y(0)\{1 + x/L_s\}$, we find that the variation of $L_\parallel(x) \approx L_\perp/|b_y(x)|$ within unstable region is about $\delta L_\parallel \approx (a/2)(L_\perp/L_s) \ll L_\parallel$ (we assume here that $L_\parallel \approx L_s \approx 1$ m). But, taking into account that the effective parallel wave number $(k_\parallel^2)_{\text{eff}} = |b_y \eta_{(\pm)} + ib_z k_n|^2$ is sensitive to the value of $\eta_{(\pm)}$, which almost cancels the large term $ib_z k_n$ (recall expression (20)), we find that magnetic shear can be important. To estimate an impact of magnetic shear, we assume that the effective value of $\eta_{(\pm)}$ is determined at

$x = 0$ and is given by Eq. (20) so that $\eta_{(\pm)} = -i(b_z(0)/b_y(0))k_n + i\delta_m k_m$. Then, we find

$$(k_\parallel^2)_{\text{eff}} \approx |\{x/[b_y(0)L_s]\}k_n + \delta_m k_m|^2. \quad (30)$$

Thus, from Eq. (30), one sees that a strong increase in the effective parallel wave number, caused by magnetic shear and resulting in the reduction of the growth rate, starts at

$$|k_n/(b_y k_m)| \gtrsim |k_\perp/k_\parallel|_{\text{sh}} \equiv 2L_s/a. \quad (31)$$

We notice that for the parameters of interest, $|k_\perp/k_\parallel|_{\text{sh}} < |k_\perp/k_\parallel|_{\text{max}}^{(A)}$ and the maximum growth rate, γ_{max} , is, actually, determined by the magnetic shear effect, which gives

$$\gamma_{\text{max}} \approx (2L_s/a)|\omega_\sigma| \sim 10^5 \text{ s}^{-1}. \quad (32)$$

Assuming $|k_\parallel|_{\text{sh}} \approx 2\pi/L_\parallel$, we find the low bound of the current convective instability wavelength $|\lambda_\perp|_{\text{sh}} \approx (a/2)(L_\parallel/L_s) \sim 1$ cm. Thus, we find that the development of the current convective instability is limited within the range of wave numbers $|k_\perp|_{\text{thr}} \lesssim |k_\perp| \lesssim |k_\perp|_{\text{sh}}$ and the growth rates $\alpha_e(2\pi/L_\parallel) \lesssim \gamma \lesssim (2L_s/a)|\omega_\sigma|$ by parallel electron heat conduction and magnetic sheath effects.

IV. CONCLUSIONS

Thus, we see that the asymmetry of the inner and outer divertors, which cause the inner divertor to detach first, while the outer one is still attached, results in the large temperature difference between the vicinities of the inner and outer targets and the onset of large electric potential drop through detached plasma of the inner divertor. This large potential drop along with inhomogeneity of the resistivity of detached plasma across the divertor leg drives the current convective instability in the inner divertor. This instability causes the fluctuations of plasma pressure in the detached plasma along the magnetic field lines, which result in bursts of plasma flow from the radiation region beyond the detachment front down to the divertor targets and, therefore, subsequent fluctuations of radiation losses similar to that observed in experiments.³ Assuming that in a nonlinear regime, the characteristic angular frequency of plasma parameter fluctuations is of the order of the growth rate of current convective

instability ($\sim 10^4\text{--}10^5\text{ s}^{-1}$), we find a reasonable agreement with experimental data showing $\sim 10\text{ kHz}$ oscillation frequency of the radiation loss. Once the outer divertor also detaches, the temperature difference between the vicinities of inner and outer targets disappears and the driving force for the current convective instability, causing the oscillation of radiation losses, vanishes. This feature is indeed observed in experiments.³

ACKNOWLEDGMENTS

This material is based upon work supported by the U.S. Department of Energy, Office of Science, Office of Fusion Energy Sciences under Award No. DE-FG02-04ER54739 at UCSD.

¹ITER Physics Basis Editors, "Chapter 4: Power and particle control," *Nucl. Fusion* **39**, 2391 (1999).

²A. G. McLean, A. W. Leonard, M. A. Makowski, M. Groth, S. L. Allen, J. A. Boedo, B. D. Bray, A. R. Briesemeister, T. N. Carlstrom, D. Eldon, M. E. Fenstermacher, D. N. Hill, C. J. Lasnier, C. Liu, T. H. Osborne, T. W. Petrie, V. A. Soukhanovskii, P. C. Stangeby, C. Tsui, E. A. Unterberg, and J. G. Watkins, *J. Nucl. Mater.* **463**, 533 (2015).

- ³S. Potzel, M. Wischmeier, M. Bernert, R. Dux, H. W. Muller, A. Scarabosio, and ASDEX Upgrade Team, *Nucl. Fusion* **54**, 013001 (2014).
- ⁴D. Carralero, G. Birkenmeier, H. W. Muller, P. Manz, P. deMarne, S. H. Muller, F. Reimold, U. Stroth, M. Wischmeier, E. Wolfrum, and ASDEX Upgrade Team, *Nucl. Fusion* **54**, 123005 (2014).
- ⁵H. J. Sun, E. Wolfrum, T. Eich, B. Kurzan, S. Potzel, U. Stroth, and ASDEX Upgrade Team, *Plasma Phys. Controlled Fusion* **57**, 125011 (2015).
- ⁶I. H. Hutchinson, *Nucl. Fusion* **34**, 1337 (1994).
- ⁷S. I. Krasheninnikov, *Phys. Plasmas* **4**, 3741 (1997).
- ⁸R. D. Smirnov, A. S. Kukushkin, S. I. Krasheninnikov, and A. Yu. Pigarov, *Phys. Plasmas* **23**, 012503 (2016).
- ⁹B. B. Kadomtsev and A. V. Nedospasov, *J. Nucl. Energy, Part C* **1**, 230 (1960).
- ¹⁰H. P. Furth, J. Killeen, and M. N. Rosenbluth, *Phys. Fluids* **6**, 459 (1963).
- ¹¹B. A. Carreras, P. W. Gaffney, H. R. Hicks, and J. D. Callen, *Phys. Fluids* **25**, 1231 (1982).
- ¹²A. B. Hassam and J. F. Drake, *Phys. Fluids* **26**, 133 (1983).
- ¹³B. B. Kadomtsev and O. P. Pogutse, in *Reviews of Plasma Physics*, edited by M. A. Leontovich (Consultants Bureau, New York, 1970), Vol. 5, p. 249.
- ¹⁴G. M. Staebler and F. L. Hinton, *Nucl. Fusion* **29**, 1820 (1989).
- ¹⁵A. V. Nedospasov, V. G. Petrov, and G. N. Fidel'man, *Nucl. Fusion* **25**, 21 (1985).
- ¹⁶H. Berk, D. D. Ryutov, and Yu. A. Tsidulko, *Phys. Fluids B* **3**, 1346 (1991).